Fundamentals of the high-shear pelletisation process

Ramaker, Johanna

Chapter 2

Nucleation stage of the high-shear pelletisation process

Abstract

A detailed description is given of the nucleation stage of the high-shear pelletisation process. Colour experiments were performed in order to describe the distribution of coloured binder liquid over the powder bed during the liquid addition stage. Based on these experiments the destructive nucleation growth mechanism is defined. Pelletisation starts with the formation of large primary nuclei. Small secondary nuclei are formed due to break-up of the primary nuclei. The formation of the primary nucleus coincided with an increase in the energy input. This nucleation process is described by the comparison of the theoretical tensile strength of the nuclei and the dynamic impact pressure. Due to densification, the secondary nuclei become stronger and growth proceeds exponentially by coalescence. The experiments suggest that the exponential growth depends linearly on the specific liquid addition rate and the impeller speed. During the kneading stage, net growth diminishes until a steady state is observed. The mean pellet size does not change during the final stages of the kneading phase resulting in a well-defined product.

This chapter is based on:

Vonk, P. Guillaume, C.P.F. Ramaker, J.S., Vromans, H., Kossen, N.W.F., Int.J.Pharm., 1997 (157): p. 93-102.

2.1. Introduction

During the last few decades, much research has been done on granule growth mechanisms. A pioneer in the investigations in granule growth mechanisms was the study of Newitt and Conway-Jones[1]. These authors precisely described the granule growth mechanisms of moistened sand in a rotating drum. They divided the granule growth into several steps, starting with nucleation, followed by crushing and layering, and coalescence. The different stages of granule growth were followed with colour experiments. This research led to the fundamental basis of the description of the mechanisms of granule growth.

Since Newitt and Conway-Jones, many researchers have described the granule growth in different apparatus and with different materials. Granulation in different apparatus results in different granules. For example: the shear forces, geometric dimensions, liquid addition method and processing time can be varied between the apparatus, resulting in more or less densified granules with different size distributions. Consequently, for the understanding of the granule growth mechanisms in each type of apparatus, one has to perform experiments based on work done before.

The aim of this study is to investigate nucleation and growth of pellets during the liquid addition and kneading phase of the pelletisation process in two different scales of Collette Gral.

2.2. Theoretical considerations

The pelletisation process consists of four stages:

1. dry mixing stage, in which premixing of the solids occurs
2. liquid addition stage,
3. wet massing stage, in which kneading of the wetted mass occurs,
4. drying stage.

Growth of granules and pellets, which occurs during the liquid addition stage and the kneading stage, has been studied to a large extent[2-4]. Usually drum and pan granulations have been investigated. These theories of the mechanisms of growth can not be translated directly to high-shear pelletisation, because among other things, the physical circumstances are quite different due to the high-shear forces present.

To understand the mechanisms of growth involved during the pelletisation process, it is necessary to know the influence of the process variables. Many authors described the influence of the liquid content and the process time on granule growth[5-8]. These studies are often restricted to the removal of fines, the pellet growth during the kneading phase and optimisation of the process by factorial design. So far, a precise understanding of the underlying mechanisms and subsequent control over the process are still a topic of great interest[9].

Coloured binder liquid can be used for the qualitative description of the distribution of the binder liquid over the bowl content and for the identification of different growth mechanisms during pelletisation. Different growth mechanisms can be clarified using coloured binder liquid, because varying colour patterns on a cross-sectional area of the pellets indicate different growth mechanisms of the pellets.

Schæfer and Mathiesen[4] described two nucleation mechanisms for melt pelletisation, i.e. immersion and distribution, depending on the ratio between the initial particle size and the binder droplet size. Sastry and Fuerstenau[10] described the nucleation of particles due to collisions between particles with a wetted surface. Here, firstly the wetting of the particles occurs (in most studies, wetting already has occurred because of the moistened feed materials used in these experiments) and secondly the collision between the wetted particles. After the nuclei are formed, further growth by coalescence and layering (or snowballing) takes place.

2.3. Materials and methods

Microcrystalline cellulose (Avicel PH101, FMC, Wallingstown, Ireland) and lactose (Pharmatose 200 mesh, DMV, Veghel, The Netherlands) were used as starting materials. Demineralised water was used as binder liquid (surface tension 0.072 $N \cdot m^{-1}$). Two commercially available Gral vertical high-shear mixers (Collette, Wommelgem, Belgium), Gral 10 (8 litre, impeller diameter 24 cm) and Gral 25 (25 litre, impeller diameter 36 cm), were used for the preparation of pellets. The Gral 10 was equipped with strain gauges attached to a computer, to measure the torque on the impeller shaft. The Gral 25 was equipped with a power consumption meter, measuring the power consumption of the impeller motor.

To study the different mechanisms of pelletisation in high-shear mixers, the following experiments were performed.

The first set of experiments examined the growth of the pellets during the pelletisation of equal amounts of MCC and lactose with water. Table 2.1 gives the formulation and some of the relevant material properties used.

Table 2.1. Formulation and material properties used during pelletisation.

material	amount (kg) Gral 10	amount (kg) Gral 25	ρ_s (kg/m^3)	d_{gw} (μm)
MCC	0.4	1.25	1608	63
lactose	0.4	1.25	1540	45
water	0.43	1.25	1000	

The liquid addition rate was set to 82 g/min by means of a peristaltic pump (type 5040, Watson Marlow ltd.) and supplied by a nozzle (BLM 9 60, Delevan 1/8). The mean droplet

size was about 5 mm.

The impeller of the Gral 10 (Gral 25) was set at 430 rpm (276 rpm) during the liquid addition stage, and chopper was set at 3000 rpm for both granulators. In this way, the tip velocities of the impellers were kept constant at 5.2 m/s and a dynamic similarity between the two mixers was obtained. The wet mass was subsequently kneaded for 15 minutes. During the kneading stage the chopper was switched off. An additional experiment was performed in the Gral 10 at an impeller speed of 650 rpm during the kneading stage. All pellets were tray-dried for 24 hours at 60°C.

The pellet size distribution was measured at different stages during the liquid addition and kneading stage. Each size distribution measurement was done with a new batch. The size distribution of the starting materials (d_{pp}) and the pellets (d_p) were measured by means of laser diffraction analysis using a Malvern 2600 laser diffraction apparatus using an 18 mm beam expander, a 1000 mm lens, and a dry powder feeder. Also the porosity of some pellets prepared in the Gral 10 was determined using an Autopore II (9220 v3.00) mercury porosimeter.

The influence of the impeller speed (varying between 60 and 600 rpm) on the dimensions of the nuclei in the Gral 10 was investigated, by preparing separate nuclei using indigotine t132 as colouring agent dissolved in the binder liquid (concentration 0.33 g/l). The coloured binder liquid was added in one minute with a nozzle (82 gram binder liquid) after which the process was stopped. The distribution of the coloured binder among the bowl content directly after the liquid addition was qualitatively investigated. The wet nuclei were sampled, and the dimensions and weights of the dry and wet nuclei were measured. Also, the dimensions of the core and the shell were measured on the cross-sectional area of the wet nuclei. From these data, the strength of the wet nuclei could be calculated using equation 2.2.

2.4. Results and discussion

2.4.1. Growth of pellets

Growth of pellets was investigated by means of the pellet size, in which 10 % (d_{10}), 50 % (d_{50}) and 90 % (d_{90}) of the volumetric pellet size distribution is smaller than the given value. The d_{10}, d_{50}, d_{90}-values of the Gral 10 and Gral 25 at different processing times are given in figure 2.1 and figure 2.2 respectively. Figure 2.3 gives the growth of pellets at different amounts of binder liquid.

The characteristics of the pellet growth in both mixers are rather similar. Initially minor growth occurs, which is demonstrated by the horizontal lines of the growth curves. After 3 minutes of liquid addition for the Gral 10 (7.5 minutes for the Gral 25), the amount of largest particles increases, which can be seen at the d_{90}-value. This corresponds to the addition of 0.2 g/g binder liquid, as can be seen in figure 2.3.

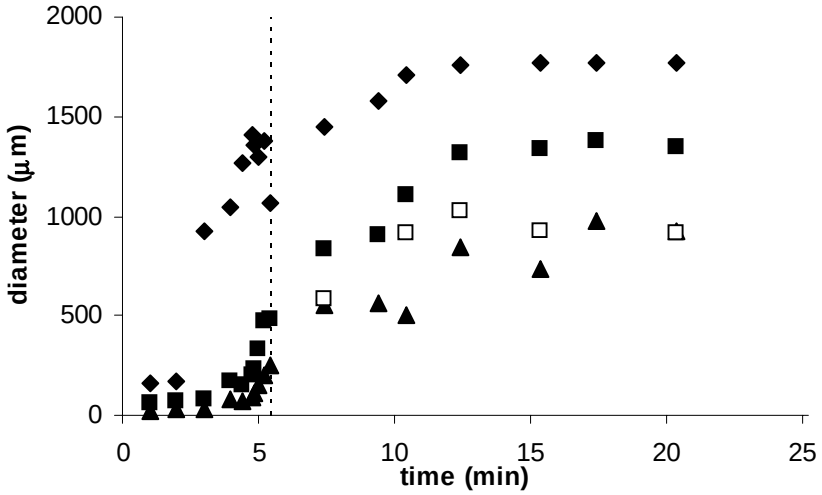

Figure 2.1. Growth of pellets in the Gral 10 at an impeller speed of 430 rpm. Key: (▲) d_{10}*;* (■) d_{50}*;* (◆) d_{90}*; and* (□) d_{50} *of the Gral 10 at an impeller speed of 650 rpm during the kneading stage. End of liquid addition at 5:25 minutes is given with the dotted line.*

Growth of the small- and medium-ranged particles starts after 4 and 10 minutes of liquid addition for the Gral 10 and Gral 25, respectively (after the addition of approximately 0.3 g/g binder liquid). Liquid addition is stopped after the addition of 0.5 gram liquid per gram solid. If more liquid would be applied, overwetting of the solid mass will occur. The amount of applied liquid thus has to be controlled within a specified range.

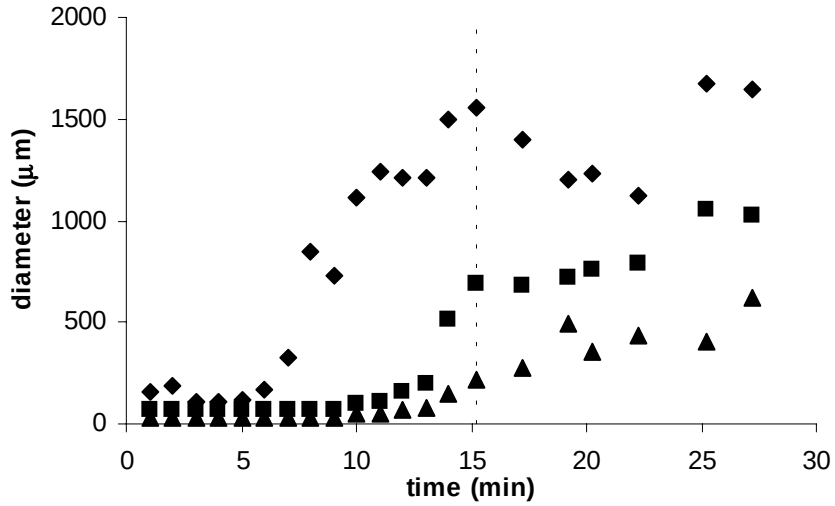

Figure 2.2. Growth of pellets in the Gral 25. Key: (▲) d_{10}*;* (■) d_{50}*;* (◆) d_{90}*. End of liquid addition at 15:15 minutes is given with the dotted line.*

Exponential growth of pellets is observed at the end of the liquid addition stage and the beginning of the kneading stage. Growth of pellets in the Gral 10 at a binder liquid content of 0.45 g/g seems to be somewhat delayed. This is probably caused by adhesion of wet material to the impeller and the wall of the Gral 10. Therefore, relatively less binder liquid is available

to cause pellet growth.

After the liquid addition stage, a 15 minutes period of kneading was applied. Here a distinct difference between the two mixers can be seen. The pellets in the Gral 10 still grow considerably, while the growth of pellets in the Gral 25 diminishes. This is mainly caused by the different amount of total liquid applied to the powder mass. In the Gral 10, an extra amount of 7.5 % binder liquid was added to the powder mass. Due to this additional 7.5 % binder liquid, the mean pellet size increases with approximately 35 %. This again shows the large influence of the liquid content.

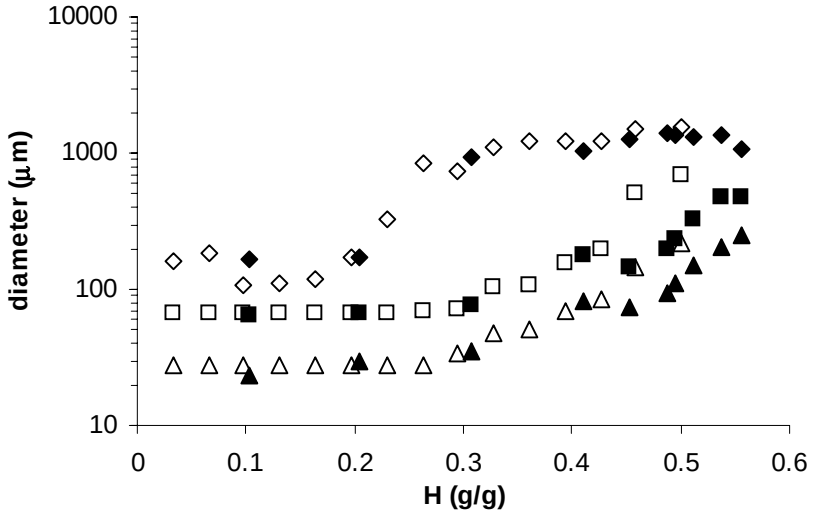

Figure 2.3. Growth of pellets as a function of the liquid contents. Key: (▲, △) d_{10}; (■, □) d_{50}; (◆, ◇) d_{90}. *The closed symbols are Gral 10-data, open symbols are Gral 25-data.*

Higher impeller rotational speed in the Gral 10 during the kneading stage results in a smaller d_{50}-value (see figure 2.1). The net growth of the pellets seems to have stopped during the final stages of the kneading phase. Usually granulation is ended while the mean granule size still increases[3,11,12]. This requires accurate control of the process because of the risk of overwetting and overgrowing of the pellets. Due to the non-changing pellet size distribution after 15 minutes of kneading, the endpoint determination is less critical in our process.

2.4.2. Small-scale experiments

2.4.2.1. Dimensions of the nuclei

The small-scale experiments in the Gral 10 were performed to characterise the nuclei during the first minutes of the liquid addition stage. Immediately after one droplet reaches the powder bed, it will adsorb powder and form a nucleus (immersion mechanism[4]). Because of the wet surface of the nucleus, particles adhere to the nucleus and cause growth by layering. As long as the outer surface of the nucleus still is wetted, growth by layering proceeds, resulting in the formation of the shell due to capillary suction[13].

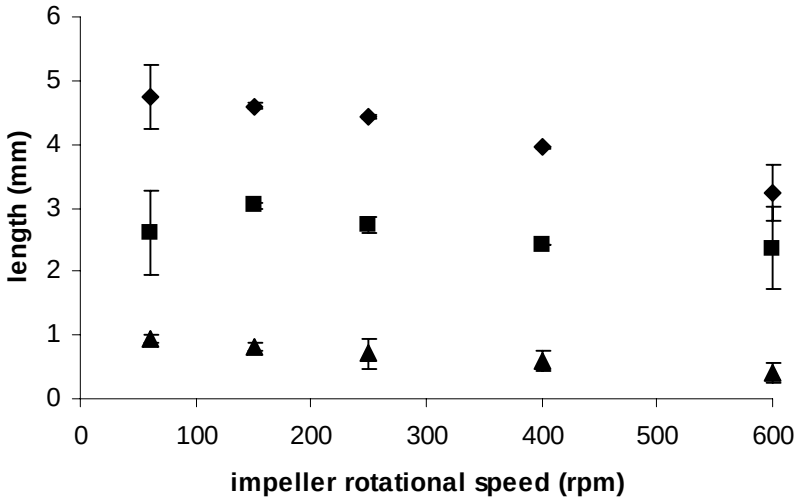

Figure 2.4. Relationship between the dimensions of the primary nucleus and the impeller rotational speed; (◆) *total radius nucleus;* (■) *radius core nucleus;* (▲) *length shell. Data points are mean of five measurements, including the standard deviation.*

The dimensions of the nuclei, prepared in the Gral 10, are given in figure 2.4 and table 2.2. All nuclei were coloured in the core, while the outer shell was less coloured or nearly uncoloured.

The size of the core and shell varied depending on the impeller rotational speed (see figure 2.4). Smaller nuclei were found at higher impeller rotational speeds. This can be seen in the decreasing size of the core and the outer shell of the nuclei. The size of the outer shell relatively decreases more compared to the size of the core of the nucleus. Also, the core of the nucleus consists of more liquid compared to the shell of the nucleus, which could be seen clearly by the large amount of colour in the core of the nucleus. The strength of the agglomerates relates linearly with the moisture content, and thus the amount of colour (see equation 2.2 and 2.3). These findings indicate that the strength of the shell is less than the strength of the nucleus.

2.4.2.2. Strength of the nuclei

The porosity of the nucleus (ε) can be estimated with the following equation:

$$\varepsilon = 1 - \frac{m_s / V}{\rho_s} \qquad (2.1)$$

where m_s is the mass of solids in the nucleus, V is the volume of the nucleus, and ρ_s is the density of the solids. With an initial droplet size of 4.7 mm the porosity of the nucleus at 600 rpm was equal to 0.63 (see table 2.2). This porosity corresponds with the bulk porosity of the powder mixture (which is about 0.6). The tensile strength of the nuclei can be calculated with the formula of Rumpf for the static tensile strength[14]:

$$\sigma_t = 8S\left(\frac{1-\varepsilon}{\varepsilon}\right)\frac{\gamma_l \cos(\theta)}{d_{pp}} \tag{2.2}$$

Here σ_t is the tensile strength of the nucleus, γ_l the surface tension of the binder liquid, θ the angle of contact between the liquid and the solid ($\theta \sim 0°$), and d_{pp} the mean primary particle size of the starting material. The saturation (S) is given by:

$$S = H\frac{1-\varepsilon}{\varepsilon}\frac{\rho_s}{\rho_l} \tag{2.3}$$

Here H is the moisture content, calculated as the ratio of the mass of the liquid and the mass of the solids, and ρ_l is the density of the liquid.

The static tensile strength of the primary nuclei is in the order of several kPa (see table 2.2).

Table 2.2. Physical properties of the nuclei prepared in the Gral 10 at varying impeller rotational speeds.

	60 rpm	150 rpm	250 rpm	400 rpm	600 rpm
m (g)	0.20	0.19	0.17	0.14	0.08
V_{tot} (ml)	0.45	0.42	0.37	0.26	0.14
V_l (ml)	0.09	0.05	0.08	0.06	0.05
ε (-)	0.72	0.72	0.71	0.67	0.63
S (-)	0.20	0.15	0.22	0.24	0.39
σ_t (kPa)	0.72	0.52	0.82	1.09	2.16

The solubility of lactose and the swelling properties of MCC make the use of the tensile strength formula of Rumpf somewhat questionable. Lactose dissolves in the binder liquid, lowers the surface tension, increases the viscosity and influences the porosity. The cellulose absorbs large amounts of water, lowers the amount of lactose which can dissolve. A strong indication of this can be found when scanning electron microscopic pictures are investigated of the pellets before and after the dissolution of the lactose from the pellets. The lactose crystals are clearly visible while the original structure of the cellulose particles can no longer be recognised. Nevertheless, the order of magnitude of the tensile strength is used to compare the tensile strength of the nuclei with the impact of the impeller.

2.4.2.3. Description of the bowl content

Besides the dimensions of the nuclei, also the distribution of the fragments of these nuclei in the bowl content was observed. The results of the distribution of the colour inside the Gral 10 are given in table 2.3. At a low impeller speed large primary nuclei are formed with a dark blue core and a white shell, which do not break in the mixer. At impeller speeds of 150 rpm and higher, the large (primary) nuclei are broken into smaller (secondary) nuclei of about 2 mm. These secondary nuclei can be identified by the light-blue colour. The size of the

secondary nuclei decreases at increasing impeller speeds. At an impeller speed of 400 rpm breakage of the primary nuclei is nearly complete because only some large (primary) nuclei and many small (secondary) nuclei are found. Breakage of the primary nuclei is complete at an impeller speed of 600 rpm, when only small secondary nuclei can be recognised, and the total bowl content is coloured blue. The nucleation process, as described above at 400 and 600 rpm, results in the formation of dense secondary nuclei, and enhances the distribution of the binder liquid.

Table 2.3. Results of the nucleus formation in the Gral 10.

impeller (rpm)	σ_{impact} (kPa) (eq. 2.8)	description of the bowl content
60	0.24	large nuclei are formed with blue nucleus and white shell
150	1.48	large nuclei together with some smaller nuclei due to break-up
250	4.11	large nuclei together with some smaller nuclei due to break-up
400	10.5	some smaller nuclei and light blue colouring of powder mass
600	23.7	some smaller nuclei and more intense blue colouring of powder mass

2.4.2.4. Impact of the impeller arm

The result of the small-scale experiments can be used for the interpretation of the nucleation stage of the pelletisation process in the Gral 10.

At an impeller speed of 85 rpm the powder bed changes from a moving bed to a well-mixed bed because the gravity force (F_g) becomes equal to the centrifugal force (F_{cen}):

$$F_g = mg \tag{2.4}$$

$$F_{cen} = m\frac{(\pi ND)^2}{(\frac{1}{2}D)} \tag{2.5}$$

$$N_c = \sqrt{\frac{g}{2\pi D}} = 1.4\,\mathrm{s}^{-1} = 85\,\mathrm{rpm} \tag{2.6}$$

Here m the mass, g the acceleration due to gravity, N the impeller rotational speed, D the diameter of the bowl, and N_c the critical impeller speed. The powder bed will be moving in a chaotic, fluidised manner, and droplets will fall on to a cloud of powder particles.

To explain the breakage of nuclei, the estimated tensile strength of a primary nucleus is compared with an order of magnitude estimation of the impact pressure caused by the impact on a nucleus by the impeller. In order to calculate the impact pressure, the acceleration of the nucleus on impact has to be estimated. The acceleration (a) is estimated by:

$$a = \frac{\Delta v}{\Delta t} \approx v_{tip}\frac{v_{tip}}{d_p} \tag{2.7}$$

Better estimations of the acceleration can be found using rigorous mathematical models like the distinct element method[15,16]. When the estimated acceleration is used, the impact pressure of the impeller is given by:

$$\sigma_{impact} = \frac{F}{A} = \frac{ma}{\pi/4\, d_p^2} \approx \frac{\frac{1}{6} d_p^3}{\frac{1}{4} d_p^2} \rho_p \frac{v_{tip}^2}{d_p} = \frac{2}{3} \rho_p v_{tip}^2 \tag{2.8}$$

Here σ_{impact} is the impact pressure, F the acceleration force, A the cross-sectional area of the pellet, m the mass of the nucleus, a the acceleration of the nucleus, d_p the diameter of the nucleus, ρ_p the density of the nucleus, and v_{tip} the tip velocity of the impeller ($=\pi ND$). The impact pressure of the impeller arm is also given in table 2.3.

In figure 2.5, the strength of the nuclei (table 2.2) is compared to impact pressure of the impeller arm (table 2.3). Figure 2.5 shows that at impeller speeds between 60 rpm and 150 rpm, the impact pressure of the impeller arm is of the same order of magnitude as the tensile strength of the nuclei. In this range of impeller speeds, breakage of the primary nuclei can just be expected, which is confirmed by our observations. At higher impeller speeds, breakage of smaller nuclei takes place and distribution of the crushed fragments of these nuclei in the bowl proceeds rapidly due to the intense mixing in the Gral.

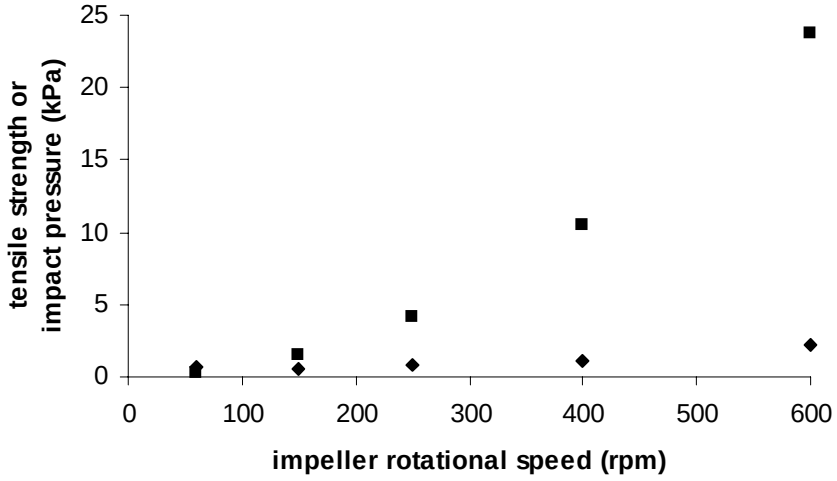

Figure 2.5. Tensile strength of the nuclei (◆) compared to the impact pressure of the impeller arm (■) at varying impeller rotational speeds.

2.4.3. Intragranular porosity

In order to characterise the pellets, mercury porosimetry was performed on dry pellets from three batches prepared in the Gral 10. The impeller speed during the kneading phase was set to 650 rpm to enhance the effect of the kneading phase. The prepared batches were taken at t = 5:15 minutes (just before the end of the liquid addition), at t = 7:25 minutes (2 minutes kneading) and at t = 20:25 minutes (15 minutes kneading). Table 2.4 gives the porosity data of the dry pellets of different sieve fractions.

Table 2.4. The porosity of the Gral 10 pellets.

Time (min)	size class (μm)	porosity†	size class (μm)	porosity†
5:15	200-500	0.117	1250-1500	0.194
7:25	200-500	0.062	1250-1500	0.081
20:25	850-1200‡	0.023	1250-1500	0.018

† porosity is calculated with the total pore volume between 0.2 μm and 10 μm.

‡ amount pellets in sieve fraction 200-500 μm was not large enough to measure the porosity.

The porosity becomes lower after intense kneading. After 20 minutes of processing, a porosity of 2 % was observed. The smaller pellets show lower porosities. The smaller pellets are probably more susceptible to densification and deformation, while the larger pellets will be more susceptible to deformation and break-up.

Decrease of the intragranular porosity is found in many different granulation processes. Pelletisation in a rotary processor of several mixtures of lactose (70-90 %) and MCC (10-30 %) results in granules with a intragranular porosity of 15-25 %[7]. In our case final porosities are found less than 10 % which is comparable with porosities found during melt pelletisation[12], and extrusion/spheronisation[17].

2.4.4. Energy input

The energy input during the pelletisation process was monitored as the torque and the power consumption profile for the Gral 10 and the Gral 25, respectively. The energy input for both apparatus, and the accompanying characteristics for the pellet size distribution are given in figure 2.6 and 2.7. In both figures, a number of different stages can be recognised.

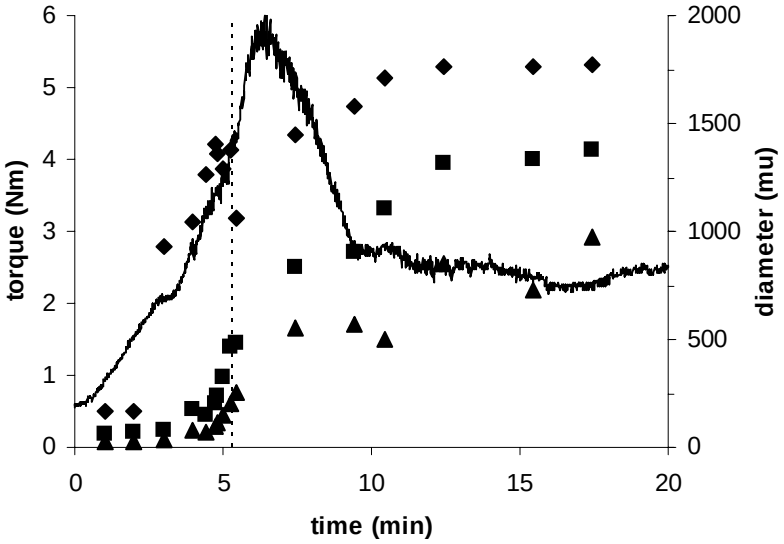

Figure 2.6. Comparison between the torque curve (—) and the pellet size distribution of the Gral 10: (▲) d_{10}; (■) d_{50}; (◆) d_{90}. *End of liquid addition is given with the dotted line.*

Firstly, during liquid addition the energy input rises steadily. The similarity between the energy input-rise and the growth of the largest particles (d_{90}) during this stage can be seen clearly in both figures.

Secondly, at the end of the liquid addition and the beginning of the kneading stage, the energy input rises until a peak value, with large amplitude variations. Growth of all particles occurs in this stage. During the moments of the fastest growth (flexion point of the pellet size distribution curves), the peak-value of the energy input curves can be observed in figure 2.6 and 2.7. During these moments, the agglomerates are formed into pellets.

The final stage starts five minutes after the end of the liquid addition stage. The energy input has dropped rapidly (within a few minutes) towards a constant value, and remains constant for at least 10 minutes. This stage corresponds to the steady state of pellet growth.

From the observations above it can be stated that growth of pellets clearly can be monitored by measuring the energy input (e.g. torque or power consumption).

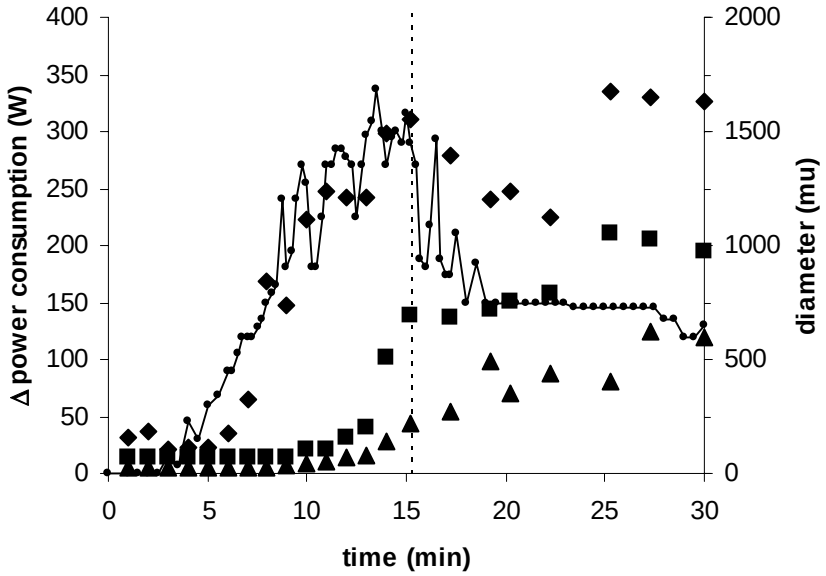

Figure 2.7. Comparison between (⁻●⁻) the power consumption curve and the pellet size distribution of the Gral 25: (▲) d_{10}; (■) d_{50}; (◆) d_{90}. End of liquid addition is given with the dotted line.

2.4.5. Definition of the growth mechanism

On the basis of our experiments we define the following mechanisms of growth (figure 2.8). The nucleation starts with one droplet. At the moment the droplet reaches the moving powder bed, a nucleus is formed. This nucleus is a loose agglomerate and can be characterised by a high porosity and a low tensile strength. The primary nucleus grows due to layering. The size of the primary nucleus is approximately 10 mm. Break-up of the nucleus proceeds according to two mechanisms.

The weak nuclei wear-off due to nuclei-nuclei and nuclei-wall collisions (abrasion), and breakage into fragments because of the action of the impeller and chopper (fragmentation).

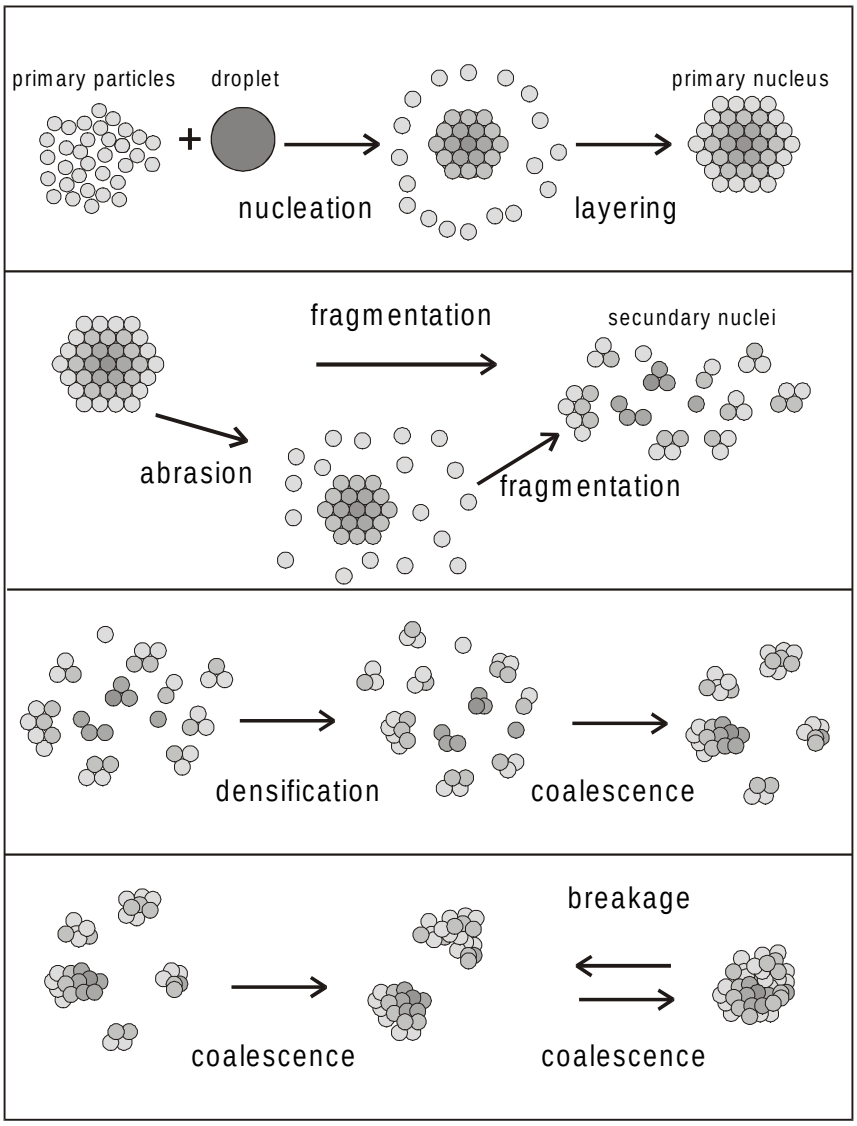

Figure 2.8. The proposed growth mechanism of high-shear pelletisation process.

Both mechanisms result in the formation of small secondary nuclei. These secondary nuclei are the starting material for the exponential growth. The exponential growth starts when the solid mass has been sufficiently wetted and densification of the secondary nuclei occurs. Due to the densification stronger pellets are formed, which survive many pellet-pellet and pellet-wall collisions. Another consequence of the densification is that liquid is squeezed to the pellet surface, which increases the coalescence probability. The exponential growth of the pellets is observed at the end of the liquid addition stage and the beginning of the kneading stage. The exponential growth can well be observed by monitoring the energy input.

During kneading, coalescence proceeds because densification still occurs (up to a porosity of 2 % at the end of the kneading stage). The growth rate decreases because no more liquid is applied, and break-up becomes more and more important. The final pellet size is limited by the destructive action of the impeller. A higher impeller speed increases the break-up of pellets and causes smaller pellets.

The proposed mechanism is not a step-wise process, but a combination of all different sub-mechanisms occurring at the same time. During liquid addition, the formation of primary and secondary nuclei is the major mechanism. The importance of the different sub-mechanisms changes during the process. Densification of the pellets becomes more important during kneading, which leads to more spherical pellets at a higher kneading time.

2.5. Conclusions

Based on the results of the experiments described in this chapter, the destructive nucleation growth mechanism of high-shear pelletisation was designed identifying nucleation, fragmentation, densification, exponential growth by coalescence, and break-up.

The early stages of the pelletisation process is characterised by the formation of large primary nuclei from single droplets, which coincides with the increase in the energy input. Fragmentation of the primary nuclei, due to the impact of the impeller and the chopper, results in the formation of small secondary nuclei. During the final stages of the liquid addition phase exponential growth by coalescence is observed, which is accompanied with a peak value in the energy input. During the kneading phase, the porosity of the dry pellets decreases to 2 %, growth of pellets diminishes, and an equilibrium stage of pellet growth of at least 10 minutes can be observed. During this stage, the energy input levels-off to a constant value.

The final pellet size depends on the impeller speed and the liquid content. At the end of the kneading stage, the pellet size distribution does not change anymore, which makes it possible to control the final pellet size.

2.6. Acknowledgement

The authors would like to thank Organon N.V. for the financial support in the instrumentation of the Gral 10.

2.7. Nomenclature

a	acceleration (m/s^2)
A	area (m^2)
d	diameter (m)
D	diameter bowl (m)
F_{cen}	centrifugal force (N)
F_g	gravity force (N)
g	acceleration due to gravity (m/s^2)
H	moisture content
m	mass (kg)
N	rotational speed (1/s)
S	saturation (-)
t	time (s)
v	velocity (m/s)
V	volume (m^3)

Greek symbols

ε	porosity (-)
γ_l	surface tension (N/m)
ρ	density (kg/m^3)
σ	strength (Pa)
θ	contact angle (deg)

Subscripts

l	liquid
p	pellet or nucleus
pp	primary particle (starting material)
s	solid
t	tensile

2.8. References

1. Newitt, D.M., Conway-Jones, J.M., A contribution to the theory and practice of granulation, Trans.Instn.Chem.Engrs. 36 (1958) p. 422-442.
2. Kapur, P.C., Fuerstenau, D.W., Size distributions and kinetic relationships in the nuclei region of wet pelletization, Ind.Eng.Chem.Process Des.Dev. 5 (1966) p. 5-10.
3. Knight, P.C., An investigation of the kinetics of granulation using a high shear mixer, Powder Technol. 77 (1993) p. 159-169.
4. Schæfer, T., Mathiesen, C., Melt pelletization in a high shear mixer. IX. Effects of binder particle size, Int.J.Pharm. 139 (1996) p. 139-148.
5. Adetayo, A.A., Litster, J.D., Desai, M., The effect of process parameters on drum granulation of fertilizers with broad size distributions, Chem.Eng.Sci. 48, 23 (1993) p. 3951-3961.
6. Newton, J.M., Chapman, S.R., Rowe, R.C., The influence of process variables on the preparation and properties of spherical granules by the process of extrusion and spheronisation, Int.J.Pharm. 120 (1995) p. 101-109.
7. Holm, P., Bonde, M., Wigmore, T., Pelletization by granulation in a roto-processor RP-2. Part I: Effects of process and product variables on granule growth, Pharm.Tech.Eur. 8, 8 (1996) p. 22-36.
8. Vertommen, J., Kinget, R., The influence of five selected processing and formulation variables on the release of riboflavin from pellets produced in a rotary processor, S.T.P.Pharma Science 6, 5 (1996) p. 335-340.
9. Ennis, B.J., Agglomeration and size enlargement. Session summary paper, Powder Technol. 88 (1996) p. 203-225.
10. Sastry, K.V.S., Fuerstenau, D.W., Mechanisms of agglomerate growth in green pelletization, Powder Technol. 7 (1973) p. 97-105.
11. Leuenberger, H., Imanidis, G., Monitoring mass transfer processes to control moist agglomeration, Pharm.Tech. , March (1986) p. 56-73.
12. Schæfer, T., Taagegaard, B., Thomsen, L.J., Kristensen, H.G., Melt pelletization in a high shear mixer. V. Effects of apparatus variables, Eur.J.Pharm.Sci. 1 (1993) p. 133-141.
13. Schaafsma, S.H., Vonk, P., Seegers, P., Kossen, N.W.F., Description of agglomerate growth, Powder Technol. 97, 3 (1998) p. 183-190.
14. Rumpf, H., The strength of granules and agglomerates, In: Agglomeration, ed. K. W.A., Interscience, New York (1962) p. 379-418.
15. Popatov, A.V., Campbell, C.S., Computer simulation of impact-induced particle breakage, Powder Technol. 81 (1994) p. 207-216.
16. Thornton, C., Yin, K.K., Adams, M.J., Numerical simulation of the impact fracture and fragmentation of agglomerates, J.Phys.D: Appl.Phys. 29 (1996) p. 424-435.
17. Vertommen, J., Rombaut, P., Kinget, R., Internal and external structure of pellets made in a rotary processor, Int.J.Pharm. 161 (1998) p. 225-236.